Supplementary Information

Organosilica nanoparticles containing sodium borocaptate (BSH) provide new perspectives for boron neutron capture therapy (BNCT): efficient cellular uptake and enhanced BNCT efficacy

Mathilde Laird,[1] Kotaro Matsumoto,[1] Yuya Higashi,[1] Aoi Komatsu,[1] Art Raitano,[2] Kendall Morrison,[2] Minoru Suzuki[3] and Fuyuhiko Tamanoi[1,4]*

[1] Institute for Integrated Cell-Material Sciences, Institute for Advanced Study, Kyoto University, Kyoto 606-8501, Japan;

[2] TAE Lifesciences, Drug Development Division, Santa Monica, CA 90404, USA

[3] Institute for Integrated Radiation and Nuclear Science, Kyoto University, Kumatori 590-0494, Japan

[4] Department of Microbiology, Immunology and Molecular Genetics, University of California, Los Angeles, USA

* Corresponding authors: tamanoi.fuyuhiko.2c@kyoto-u.ac.jp

I. BPMO synthesis and characterization

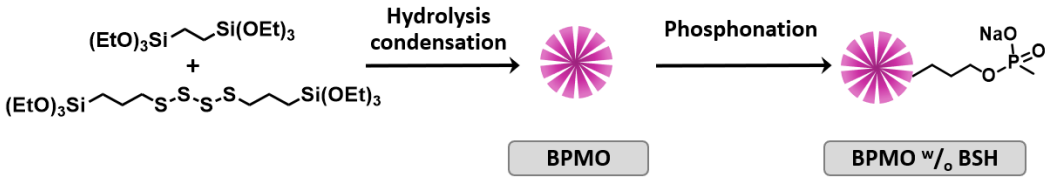

Fig. S1: BPMO $^{w}/_{o}$ BSH synthetic pathway

Sample	DLS size (nm)	Z-potential (eV)
BPMO	357	-38.0
BPMO-vinyl	362	-26.5
BPMO-vinyl-phos	343	-50.1
BSH-BPMO	351	-51.5
BPMO $^{w}/_{o}$ BSH	336	-47.8

Table S1: DLS and Z-potential characteristics of BPMO nanoparticles

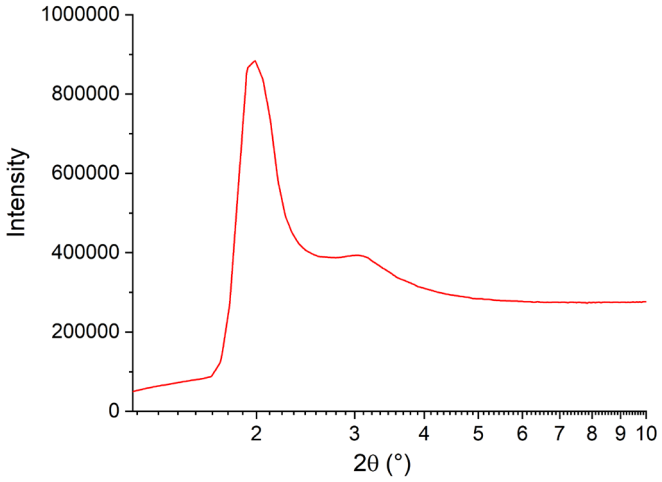

Fig. S2: Power XRD diffractogram of BPMO

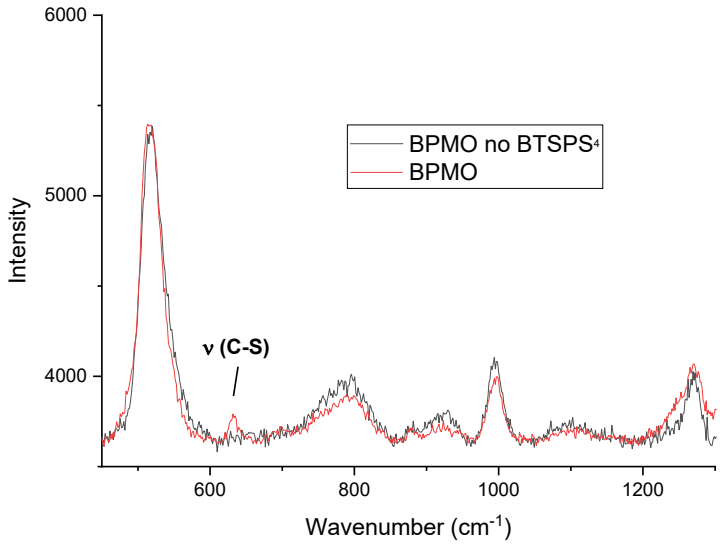

Fig. S3: Raman spectra of BPMO without and with $BTSPS_4$

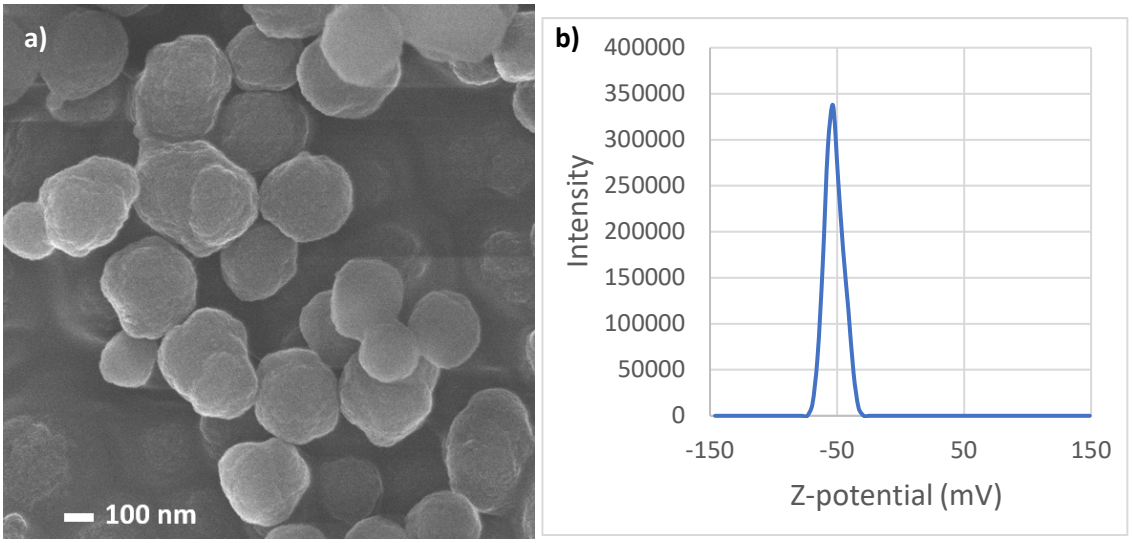

Fig. S4: SEM images of BSH-BPMO demonstrating the absence of aggregation following thiol-ene reaction (a) Z-potential of BSH-BPMO (b)

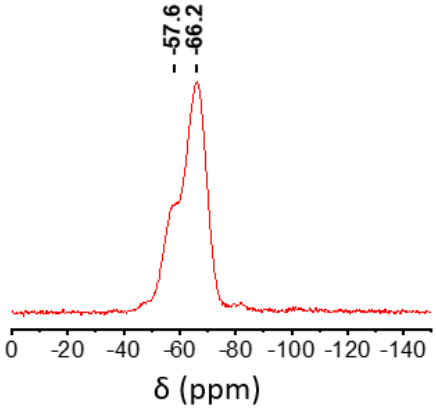

Fig. S5: ^{29}Si solid state NMR of BSH-BPMO

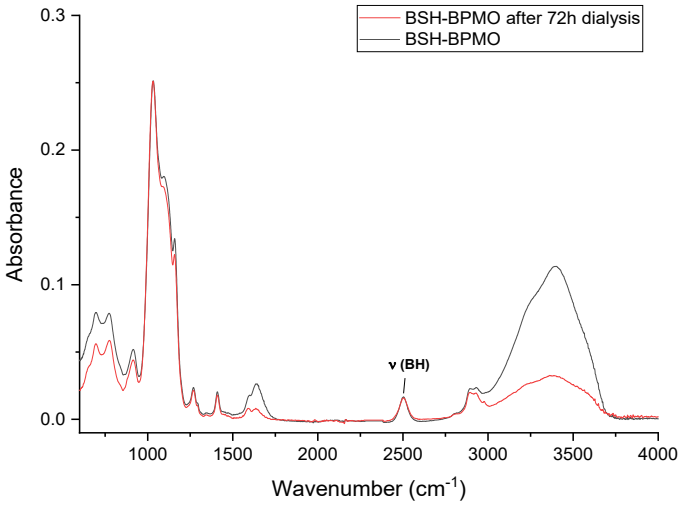

Fig. S6: FTIR spectra of BSH-BPMO and BSH-BPMO after dialysis at 37 °C for 72 h

Several washing cycles with water at 35-45 °C were performed to confirm the covalent grafting of the BSH onto the silica nanoparticles (BSH is highly soluble in water) and no significant change was observed by FTIR or by ICP. A BSH-BPMO suspension in water (14 mg in 1 mL) was also placed in a dialysis bag (5 nm size pores and molecular cut-off of 12000-14000 Da) and immersed in water (9 mL) at 37 °C for 72 h. The nanoparticles were recovered by centrifugation and dried to analyze the remaining boron content. No significant BSH release was observed by FTIR or by ICP (**Fig. S6**).

II. Cellular uptake and cytotoxicity of BSH-BPMO

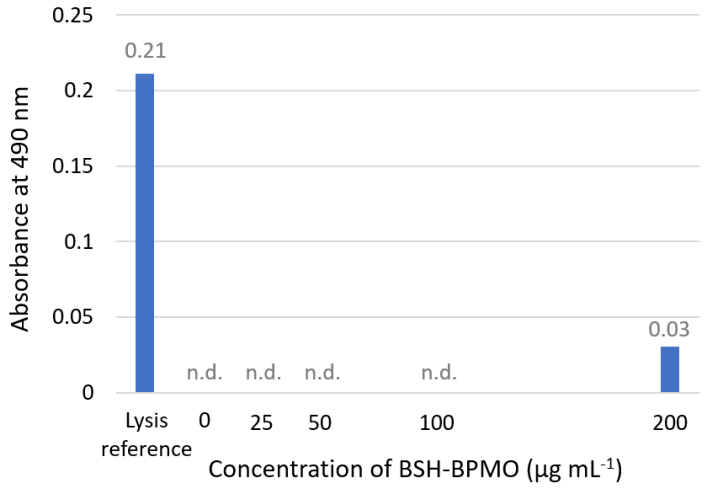

Fig. S7: Cytotoxicity of BSH-BPMO after 24h by LDH assay. n.d. = not detected

Slight cytotoxicity can be observed from 200 µg mL^{-1}.

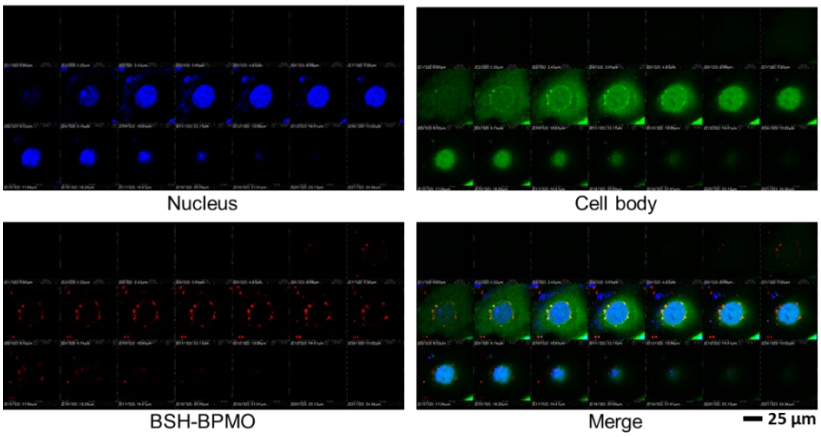

Fig. S8: Cellular uptake of BSH-BPMO in OVCAR8 cancer cell line, z-slices for 10 µg of BSH-BPMO per dish: Hoechst-dyed nucleus observed at 405 nm, GFP-expressed modified OVCAR8 cell at 488 nm and Rhodamine B containing BSH-BPMO at 561 nm

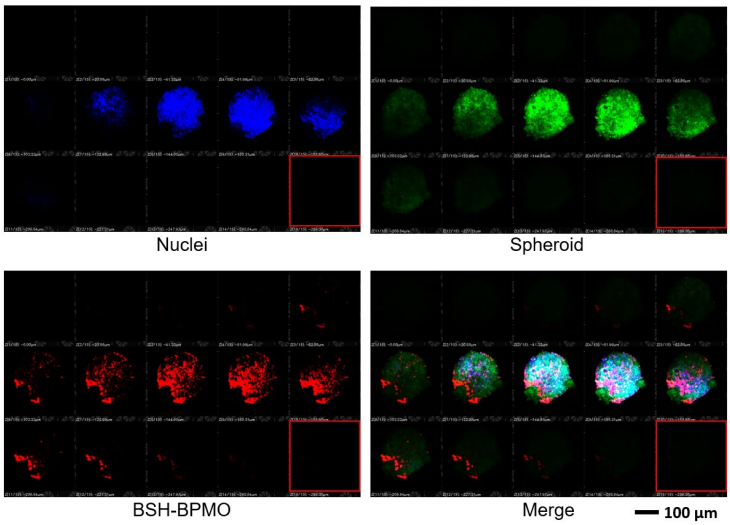

Fig. S9: Cellular uptake of BSH-BPMO in OVCAR8 spheroids, z-slices for 25 µg of BSH-BPMO per spheroid: Hoechst-dyed nuclei observed at 405 nm, GFP-expressed OVCAR8 cell at 488 nm and Rhodamine B containing BSH-BPMO at 561 nm

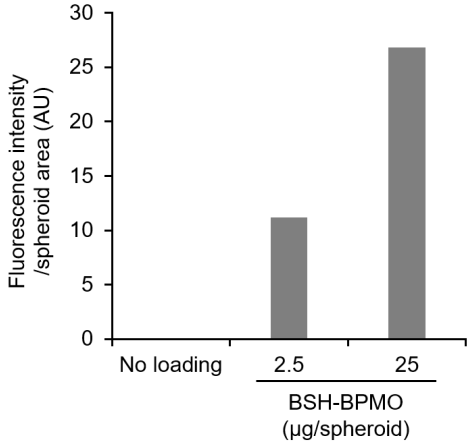

Fig. S10: Rhodamine B fluorescence intensity per area of the spheroid in the bright field.

III. Neutron exposure assay

Sample	Standard error (%)	Standard deviation (%)	p-value
No loading	5.88	10.19	-
BPMO w/o BSH	8.28	14.35	0.0125
Free BSH	5.34	9.25	0.0175
Free BPA	16.04	27.79	0.0520
BSH-BPMO	0.49	0.84	0.0025

Table S2: Statistic values for the irradiated spheroid data

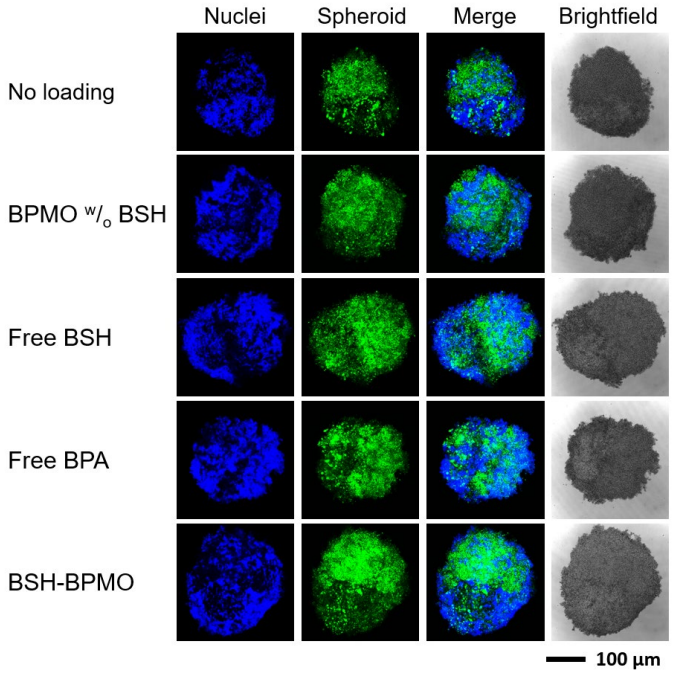

Fig. S11: OVCAR8 spheroids observed by confocal microscopy after 3 days incubation and without neutron irradiation: Hoechst-dyed nuclei observed at 405 nm, GFP-expressed OVCAR8 cell at 488 nm